

GPS total electron content variations associated with poleward moving Sun-aligned arcs

P. T. Jayachandran,¹ K. Hosokawa,² K. Shiokawa,³ Y. Otsuka,³ C. Watson,¹ S. C. Mushini,¹ J. W. MacDougall,⁴ P. Prikryl,⁵ R. Chadwick,¹ and T. D. Kelly¹

Received 29 November 2011; revised 27 February 2012; accepted 28 March 2012; published 9 May 2012.

[1] GPS total electron content (TEC) has shown quasiperiodic oscillations of varying amplitude associated with poleward moving Sun-aligned arcs. The amplitude of TEC variations showed a maximum of ~ 3 TECU and seemed to decrease as the arcs moved poleward from the source/generation region. Simultaneous DMSP data showed that fluctuations in TEC and optical intensification were caused by precipitation of high-energy (>500 eV) particles. Concurrent ionosonde observations also exhibited quasiperiodic variations (within limit of the resolution of the data) in peak ionospheric electron density of the ionosphere. Bottom height of the ionospheric layers produced by precipitating particles varied between 130 km (upper *E* region) and 300 km (*F* region), indicating variable particle precipitation energy. Frequency analysis of high-resolution TEC data showed a broad range of discrete frequency components from 1.60 mHz to 22.80 mHz present in the TEC oscillations, which may provide insight into the energization/modulation of precipitating particles by these oscillations. A broad distribution of equivalent vertical thickness of arcs was calculated using GPS TEC and ionosonde measurements of peak electron density. This distribution showed a minimum thickness of 21 km, a maximum of 84 km, and an average of 49 km. The equivalent vertical thickness also showed a linear relationship with bottomside height of the ionospheric layer (auroral arc). The relationship showed an increase in the vertical thickness with an increase in bottomside height of the layer. This relationship is a consequence of variations in the energy of the precipitating particles causing different ionospheric production profiles.

Citation: Jayachandran, P. T., K. Hosokawa, K. Shiokawa, Y. Otsuka, C. Watson, S. C. Mushini, J. W. MacDougall, P. Prikryl, R. Chadwick, and T. D. Kelly (2012), GPS total electron content variations associated with poleward moving Sun-aligned arcs, *J. Geophys. Res.*, 117, A05310, doi:10.1029/2011JA017423.

1. Introduction

[2] The Earth's high-latitude ionosphere, a region of the upper atmospheric environment, is complex in terms of electrodynamics and plasma structuring as a result of interactions in the solar wind-magnetosphere-ionosphere systems. The polar cap ionosphere is often composed of ionization structures of varying temporal and spatial scales produced by a variety of mechanisms [e.g., *Tsunoda*, 1988; *Valladares and*

Carlson, 1991; *Valladares et al.*, 1994; *Crowley*, 1996; *Basu and Valladares*, 1999; *Shiokawa et al.*, 1997; *MacDougall and Jayachandran*, 2007; *Newell et al.*, 2009a]. These mechanisms are both internally (ionospheric electrodynamics and plasma instabilities) and externally (particle precipitation, field aligned currents) driven, by processes that are often interconnected and very difficult to delineate. Irrespective of the underlying generation mechanisms, the resulting ionospheric structures can ultimately affect performance of communication and navigation systems in the polar regions. Precision monitoring of electron density structures in the ionosphere will have significant implications in almost all areas of the Global Navigation Satellite Systems such as GPS-based technologies [*Lanzerotti*, 2001; *Kintner et al.*, 2007].

[3] Optical studies of polar cap auroral forms, which are on average much weaker than auroral arcs, began during the International Geophysical Year (IGY) in both hemispheres. These studies showed the presence of strong, distinct auroral features in the auroral zone [*Davis*, 1960; *Denholm and Bond*, 1961]. Satellite-based measurements of polar cap auroral forms began in the early 1970s using ISIS 2 [*Ismail et al.*, 1977], when satellite-based particle measurements revealed they can be produced by soft electron precipitation

¹Physics Department, University of New Brunswick, Fredericton, New Brunswick, Canada.

²Department of Information and Communication Engineering, University of Electro-Communications, Tokyo, Japan.

³Solar-Terrestrial Environment Laboratory, Nagoya University, Nagoya, Japan.

⁴Department of Physics and Astronomy, University of Western Ontario, London, Ontario, Canada.

⁵Communication Research Centre, Ottawa, Ontario, Canada.

Corresponding author: P. T. Jayachandran, Physics Department, University of New Brunswick, PO Box 4400, Fredericton, NB E3B 5A3, Canada. (jaya@unb.ca)

Copyright 2012 by the American Geophysical Union.
0148-0227/12/2011JA017423

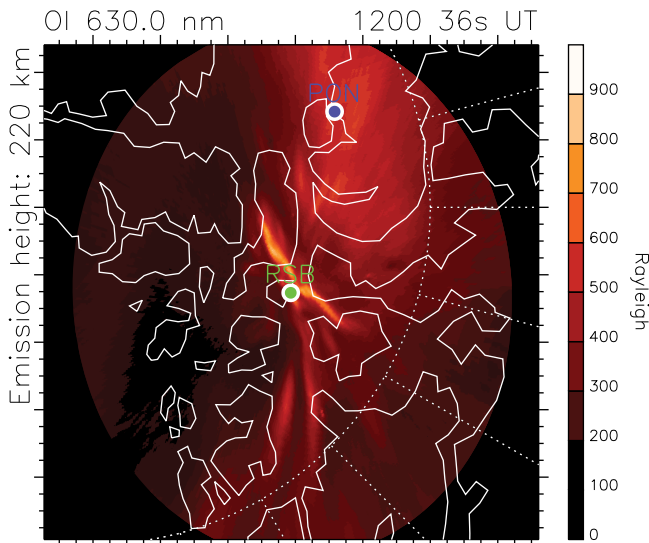


Figure 1. The 630 nm image mapped in magnetic latitude and magnetic local time coordinates assuming an emission height of 220 km. Locations of GPS stations are superposed.

[Hardy, 1984]. Further studies have revealed different types of polar cap auroral forms with distinguishable morphological features and particle signatures varying from significant ion precipitation to discrete, high-energy electron precipitation. Understanding the source region(s) precipitation, acceleration mechanism(s), and dynamics of these arcs is still an active area of research. See reviews by Zhu *et al.* [1997] for morphological features of polar cap arcs and by Newell *et al.* [2009a] for particle precipitation signatures. Ground-based studies of polar cap arcs have been primarily based on optical instruments [Sandholt *et al.*, 1990; Shiokawa *et al.*, 1996, 1997] and incoherent scatter radars [Valladares and Carlson, 1991]. Recently, GPS-based techniques have been used to study auroral arcs [Kintner *et al.*, 2002] and polar cap arcs [Jayachandran *et al.*, 2009a].

[4] One of the most prominent and dynamic forms of polar cap aurora is the poleward moving Sun-aligned arc (PMSAA), which occurs more frequently in the morning sector than the evening sector [Ismail *et al.*, 1977]. These arcs are often quasiperiodic and occur predominantly during northward interplanetary magnetic field (IMF) conditions [e.g., Shiokawa *et al.*, 1996, 1997]. Some optical forms associated with these arcs are produced by “inverted V” type electron spectra [Frank *et al.*, 1986; Shiokawa *et al.*, 1996], indicating electrostatic acceleration of precipitating particles. Recent studies have shown that dispersive Alfvén waves can also accelerate particles [Chaston *et al.*, 2004, 2007], and statistically, the location of these arcs seems to coincide with the statistical location of broadband aurora observed by DMSP particle measurements [Newell *et al.*, 2009b]. We should note that similar periodic poleward motion of auroral arcs was reported in the dayside polar cap boundary as poleward moving auroral forms (PMAFs) on the basis of optical observation at Ny-Ålesund (78.9°N, 11.9°E) [e.g., Sandholt *et al.*, 1990; Sandholt and Farrugia, 1999]. The PMAFs are observed during southward IMF. On the other hand, the quasiperiodic poleward moving Sun-aligned arcs (PMSAAs) occur during northward IMF in the

dawn sector. One of the major handicaps of ground-based optical measurements is their low cadence and thus limited ability to resolve temporal structures within these arcs. The recent establishment of high data rate GPS networks, such as the Canadian High Arctic Ionospheric Network (CHAIN) [Jayachandran *et al.*, 2009b], in the high-latitude ionosphere makes it possible to study polar cap auroral forms at high temporal and spatial resolution and to understand finer structures and dynamics of auroral forms. In this paper, we present the first ever observations of GPS total electron content (TEC) variations associated with PMSAAs. Also presented is time-frequency analysis of these TEC variations and calculations of equivalent vertical thickness of PMSAAs by using the measurements of TEC and peak electron density.

2. Data and Measurements

[5] Primary data for this study are the high data rate GPS TEC measurements from two of the 10 high data rate CHAIN GPS receivers and electron density measurements from two of the six CHAIN ionosondes. These stations are Resolute Bay (RSB) (74.75°N, 265.00°E geographic) and Pond Inlet (PON) (72.69°N, 282.04°E geographic). CHAIN GPS receivers measure GPS observables at a sampling rate of 50 Hz. However, for this study we are using 1 Hz TEC measurements because meaningful TEC variations we are dealing with are greater than 1 s time scales. TEC variations shown in the paper are slant TEC (sTEC). Canadian Advanced Digital Ionosondes (CADI) of CHAIN collect standard ionograms with 1 min cadence and fixed frequency drift at 30 s cadence. See Jayachandran *et al.* [2009b] for further details of the CHAIN instruments. We also use data from the all-sky imager (ASI) located at Resolute, a part of optical mesosphere thermosphere imagers (OMTIs) [Shiokawa *et al.*, 1999; Hosokawa *et al.*, 2006]. ASI measurements used for this study are the optical emission intensity of oxygen green and red lines at wavelengths of 557.7 and 630.0 nm, respectively. These measurements are made at 2 min intervals [Hosokawa *et al.*, 2009]. Figure 1 shows the locations of the stations in magnetic local time-magnetic latitude coordinate systems (top is to the Sun and left is to the dusk) at 12:00 UT. An ASI 630 nm image (during one of the events considered in this study), assuming an emission height of 220 km, is included in the figure in order to provide a sense of location of the GPS receivers with respect to the ASI’s field of view. It can be seen that even though the ASI is located at RSB, PON is within the field of view of the imager for the red line emission, and it is near the edge of the field of view for the green line emission. We also use solar wind (SW) and interplanetary magnetic field (IMF) measurements from the ACE and Wind satellites, as well as the OMNI database of CDAWEB (<http://cdaweb.gsfc.nasa.gov/>) to obtain the underlying interplanetary conditions during the events discussed in this paper.

3. Observations

[6] The Resolute Bay ASI, under northward IMF conditions, often detects quasiperiodic auroral forms in the morning sector. These optical forms are often Sun-aligned and move poleward. Shiokawa *et al.* [1996, 1997], using

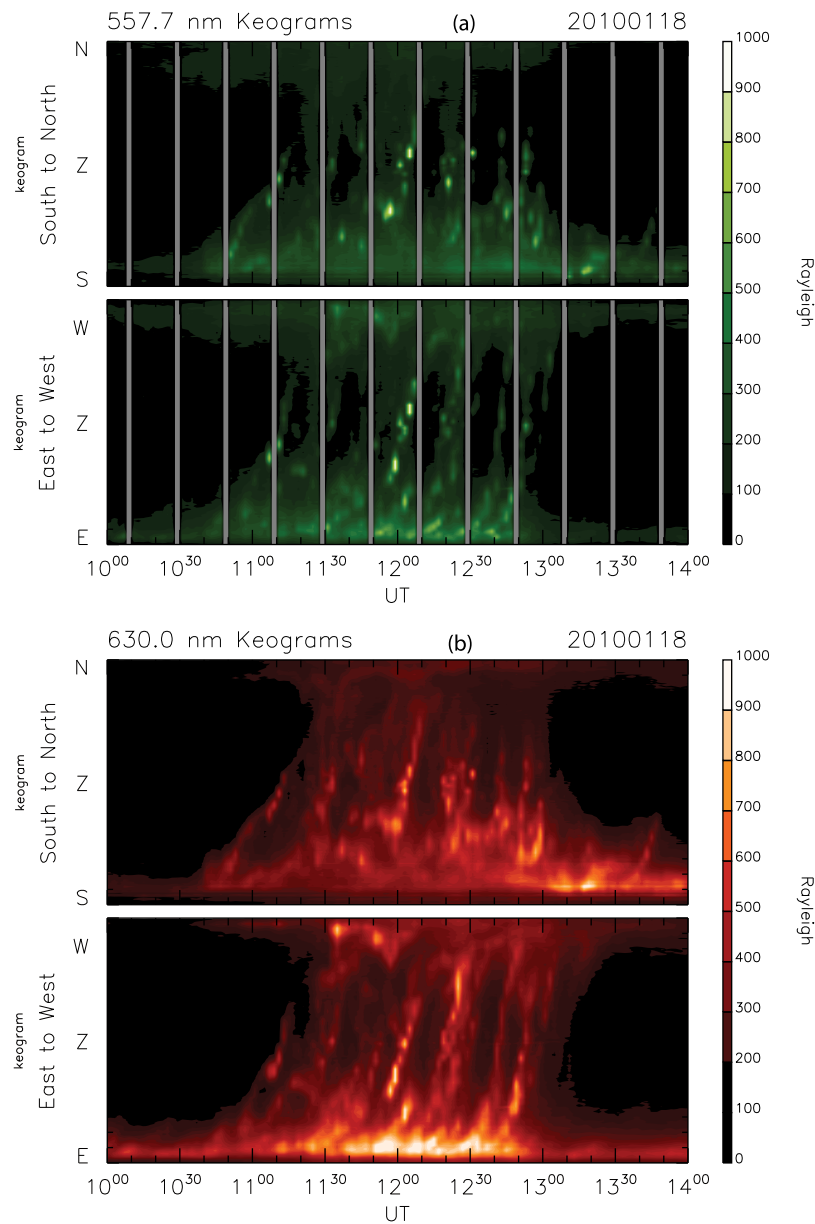
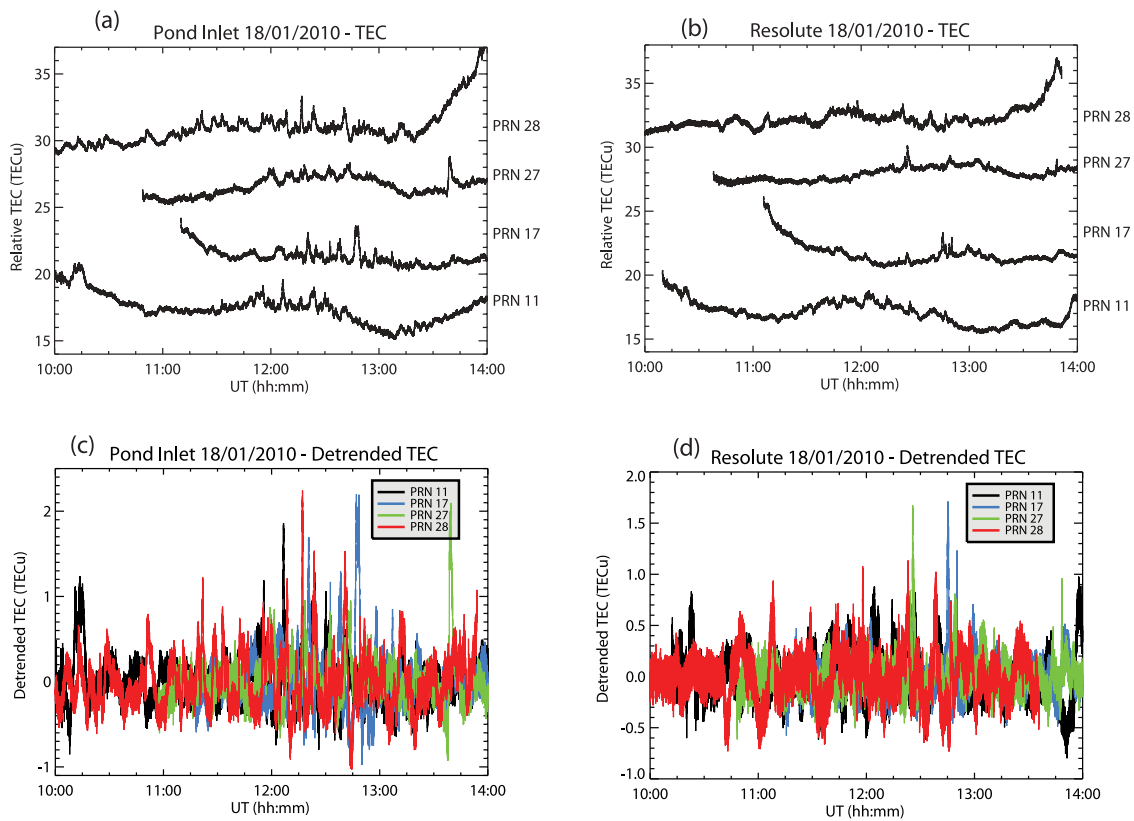


Figure 2. Optical N-S and E-W keograms generated using Resolute Bay all-sky imager (ASI) images at (a) 557.7 nm and (b) 630 nm for the period 10:00–14:00 UT of 18 January 2010. N-S and E-W tilted optical features are the poleward moving Sun-aligned arcs (PMSAAs).

measurements from another polar cap station, classified these as poleward moving Sun-aligned arcs (PMSAAs). An example keogram of such optical forms is shown in Figure 2, which shows north-south (N-S) and east-west (E-W) keograms constructed from oxygen green line (557.7 nm for Figure 2a) and red line (630.0 nm for Figure 2b) ASI images during the period 10:00–14:00 UT of 18 January 2010. Several optical features at both wavelengths started appearing after 10:30 UT and continued until 13:30 UT. These optical forms are slanted in both E-W and N-S directions, which is indicative of a poleward motion of the E-W tilted arcs. A closer examination of these optical features also reveals that they are structured and somewhat quasiperiodic. GPS TEC variations from PON and RSB during the period 10:00–14:00 UT of 18 January 2010 are

shown in Figures 3a and 3b, respectively. CHAIN GPS receivers can measure TEC from up to 10 different GPS satellites (pseudorandom numbers (PRNs)) simultaneously, providing essentially TEC measurements along 10 different satellite-to-receiver raypaths. In this study we are limiting the number of GPS raypaths by applying two simple criteria: (1) Only measurements from satellites at $>20^\circ$ elevation angles are used to significantly reduce effects of multipaths, and (2) only continuous TEC measurements for >2 h in duration from the same PRN/raypath are used. This is to get a clear time series of TEC variations due to PMSAAs and to reduce TEC variations due to spatial variation of the ionosphere and geometrical effects. These conditions limit our simultaneous TEC measurements to four different PRNs/raypaths for this event. TEC magnitudes shown in these



(e)

(e) GPS satellite IPP tracks (220 km) - 10:00 to 14:00 UT

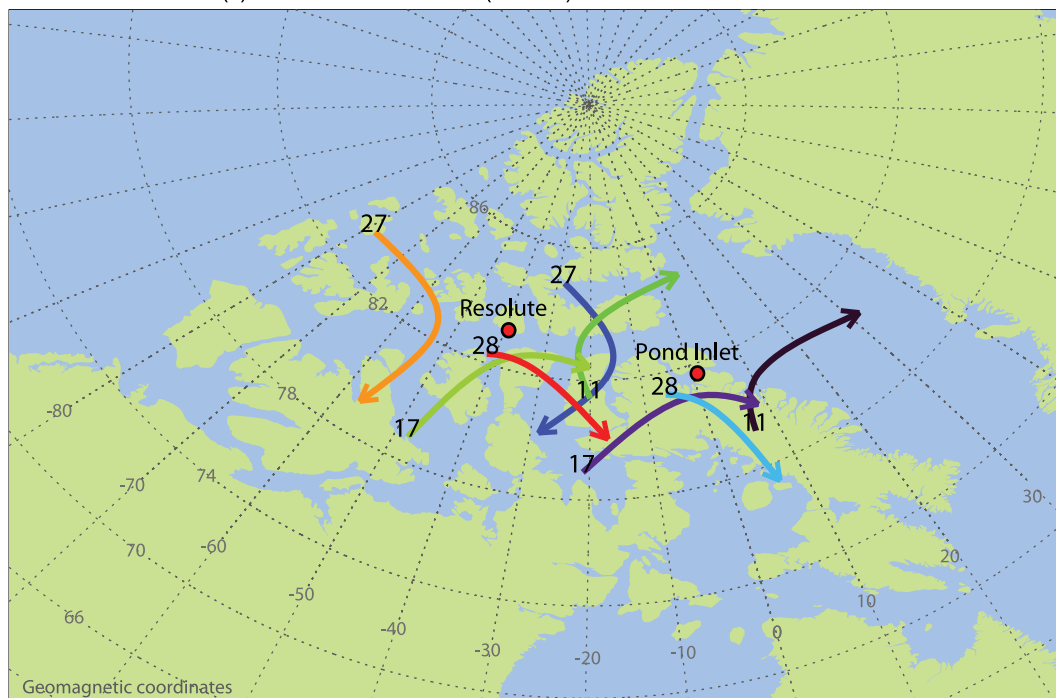


Figure 3. Variations of total electron content (TEC) measured by four GPS satellites (pseudorandom numbers (PRNs)) at (a) Pond Inlet (PON) and (b) Resolute Bay (RSB) during 10:00–14:00 UT of 18 January 2010. Detrended TEC variations at (c) PON and (d) RSB. (e) A map in geomagnetic coordinates of the ionospheric pierce point (IPP) tracks at 220 km altitude of the four GPS satellites used in Figures 3a and 3b for the same duration.

figures are relative (not absolute) because the measurements are not corrected for differential code biases (DCBs), however, the magnitude of the variations in TEC is absolute. It is evident from these figures that smaller quasiperiodic TEC oscillations/fluctuations are embedded in the larger TEC trend (due to the motion of the satellite as well as other normal/diurnal variations). In order to focus on smaller-scale TEC oscillations, we have removed this trend by applying a simple Butterworth filter that removes oscillations with a period greater than 30 min. Figures 3c and 3d, respectively, show the trend-removed TEC oscillations at PON and RSB. Quasiperiodic TEC fluctuations are visible at both stations and on all four raypaths during the optical auroral forms shown in Figure 2. The amplitude of these TEC fluctuations reached as high as ~ 3 TECU ($1 \text{ TECU} = 10^{16} \text{ e/m}^2$) at PON and ~ 2 TECU at RSB, which is quite significant. The amplitude of oscillations is higher at PON than at RSB on average since the optical aurora are formed in the vicinity of PON (inferred from the optical images). A closer examination of these fluctuations also reveals a phase difference between TEC oscillations along different raypaths, indicative of the motion of the electron density structures that are producing the TEC variations. Figure 3e shows the location of ionospheric pierce points (IPP) of different PRNs by assuming an ionospheric height of 220 km. Optical forms are moving poleward (from PON to RSB) with a slight E-W tilt, thus the observed phase differences are just due to the motion of optical forms as they intersect different raypaths at different times. Theoretically this should allow us to estimate the propagation velocity of these arcs using the GPS triangulation method described by Jayachandran *et al.* [2009a] and later extensively used by Watson *et al.* [2011]. However, due to the cumulative effects of these structures, unambiguous determination of the velocity was impossible.

[7] Another example of ASI observation of PMSAAs is shown in Figure 4 for 11:00–15:00 UT on 23 December 2009. Figure format and presentation are similar to those of Figure 2, showing N-S and E-W keograms constructed from 557.7 nm (Figure 4a) and 630.0 nm (Figure 4b) ASI images. Intense optical forms in both emissions started appearing slightly after 11:00 UT, and features are similar to the ones in the previous example with one slight difference. Some of the optical features in this case are less pronounced in the oxygen green line when compared to the red line, especially slightly after 13:30 UT. Also just after 13:30 UT, the optical features are confined to the southern edge of the ASI field of view and never cross zenith. These arcs showed a level of quasiperiodicity similar to the previous case and were again slanted in the N-S and E-W directions, indicative of moving arcs. Variations in relative TEC during the same period at PON and RSB are shown in Figures 5a and 5b, respectively. TEC variations from five GPS satellites (PRNs) or raypaths satisfied the criteria applied to the previous case. Quasiperiodic TEC fluctuations embedded in the larger trend and associated with optical features are again observed and are highlighted in the detrended TEC in Figures 4c and 4d. Fluctuations started appearing slightly after 11:15 UT, the same time as the appearance of the optical forms. In this case, the maximum amplitude of fluctuations reached as high as ~ 3.5 TECU at PON and ~ 3 TECU at RSB, with average amplitudes higher at PON. One feature that is

different in this case compared to the previous case is the change in nature of TEC fluctuations just after 13:30 UT at both stations. A sharp drop in fluctuation amplitude and frequency of occurrence is evident at both stations after 13:30 UT when compared to fluctuations prior to 13:30 UT. It is also obvious that fluctuations are more pronounced at PON than at RSB after 13:30 UT. This is consistent with the confinement of optical features to the southern edge of the field of view after 13:30 UT in Figure 4. A phase delay in oscillations between different raypaths is also evident, which is indicative of the motion of the electron density structure causing these TEC variations. Figure 5e shows IPP locations of the five different raypaths at RSB and PON, again by assuming an ionospheric height of 220 km. Closeness of IPP positions should ideally allow for calculation of PMSAA velocities, but this was also impossible due to the cumulative effects of these structures in the TEC.

4. Discussion

[8] Optical auroral forms presented in this study fit characteristics of PMSAAs described by Shiokawa *et al.* [1996, 1997] and are observed predominantly during northward IMF conditions. A case study presented by Shiokawa *et al.* [1996] showed that these arcs are produced by high-energy electron precipitation ($>450 \text{ eV}$) originating from the plasma sheet. During the events presented in this paper, the DMSP F17 satellite flew over the RSB ASI field of view. Figure 6a (18 January 2010) and Figure 6c (23 December 2009) show DMSP tracks overlaid on ASI images during each event to give contextual information of these tracks with respect to the ASI field of view and the optical features. These plots clearly show that the DMSP F17 satellite flew over the ASI's field of view for both events. Corresponding particle spectrograms measured by DMSP 17 satellites are shown in Figures 6b and 6d for 18 January 2010 and 23 December 2009, respectively. Both spectrograms show discrete accelerated electron precipitation poleward of diffuse electron precipitation as the satellite passed over a PMSAA. Electron energies were as high as 1 keV during these events, and the source region of the precipitation seems to be the boundary plasma sheet (BPS) as identified by an automated procedure based on Newell and Meng [1994] and very close to the central plasma sheet (CPS) region. However, the focus of this paper is on the ionospheric effects of the particle precipitation rather than on the magnetospheric source regions. The purpose of the DMSP observation is only to show that there were particle precipitations of significant energy. We have shown that PMSAAs are one of the mechanisms that can cause fluctuations in GPS TEC at high latitudes, although these fluctuations are small in temporal and spatial scales when compared to GPS TEC variations due to other polar region mechanisms such as Tongue of Ionization (TOIs) [e.g., Foster *et al.*, 2005] and polar patches [e.g., MacDougall and Jayachandran, 2007]. TEC fluctuations associated with PMSAAs are comparable to TEC variations due to isolated polar cap arcs [Jayachandran *et al.*, 2009a] and TEC variations generated by sudden magnetospheric compression [Jayachandran *et al.*, 2011].

[9] Both airglow emission intensity and TEC measurements are integrated quantities and will not provide any direct information on energy levels of precipitating particles

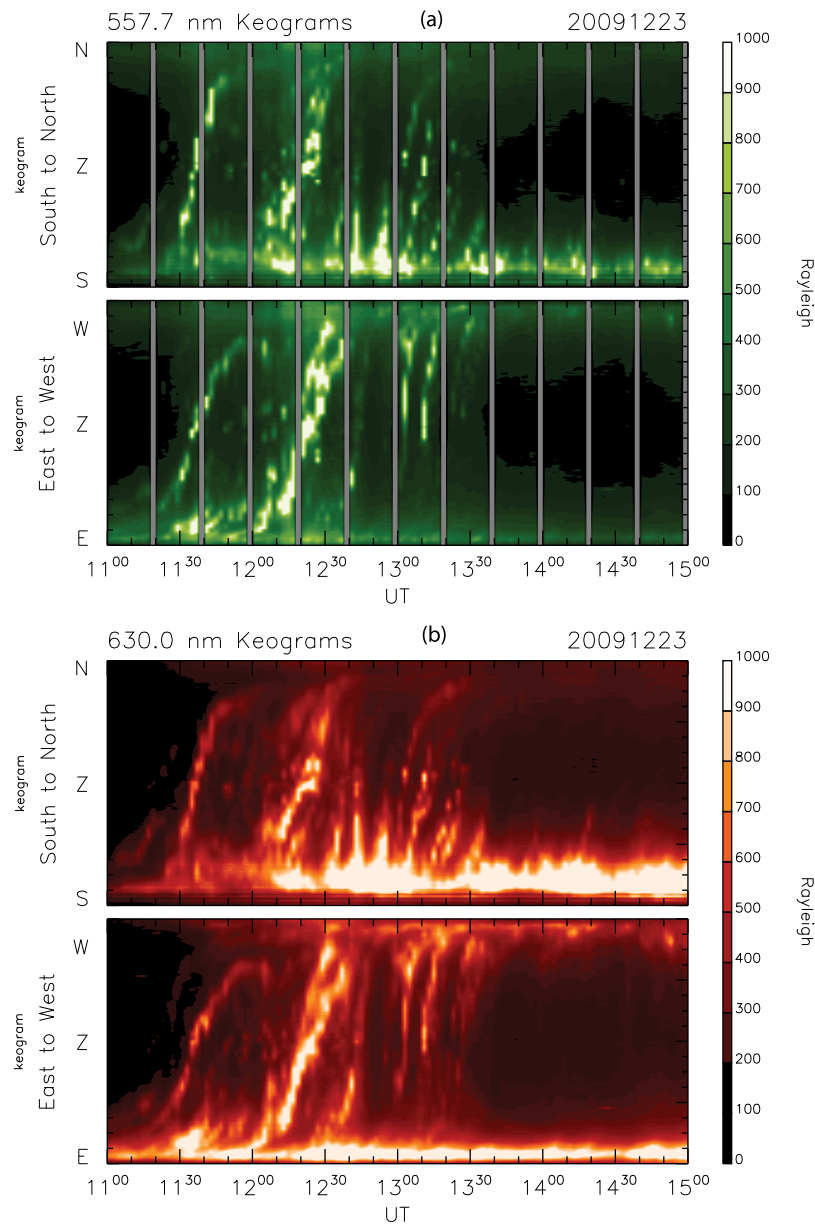
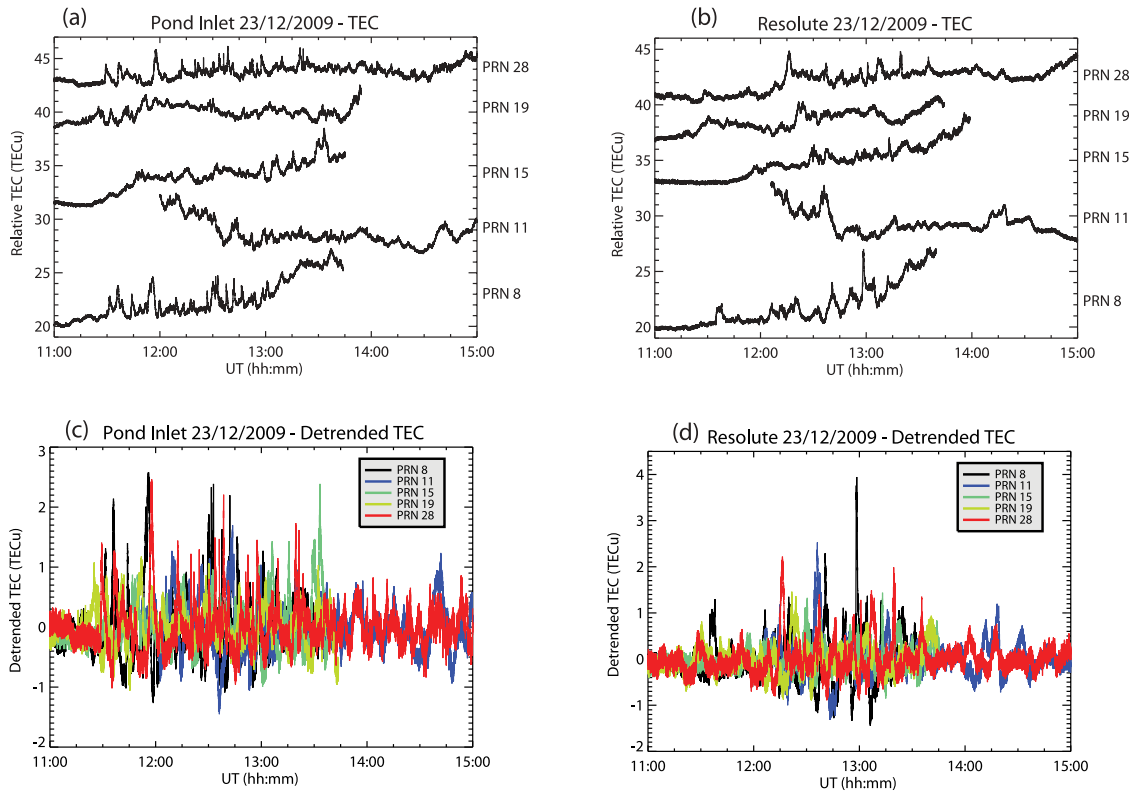


Figure 4. Optical N-S and E-W keograms generated using Resolute Bay ASI images at (a) 557.7 nm and (b) 630 nm for the period 11:00–15:00 UT of 23 December 2009. N-S and E-W tilted optical features are the poleward moving Sun-aligned arcs (PMSAAs).

in lieu of DMSP particle measurements. The presence of optical intensifications in both green and red lines suggests that precipitating particles have high enough energy to reach the *E* region of the ionosphere (~ 120 km) and produce enhanced emission at 557.7 nm. In this part of the discussion we are going to concentrate on the ionospheric consequences of these precipitating particles in terms of electron density and TEC and also on deducing some other properties of PMSAAs. Figure 7 shows the group range of four MHz reflections measured by CADIs at PON (Figures 7a and 7d) and RSB (Figures 7b and 7e), along with calculated peak electron densities (Figures 7c and 7f). The left column plots are for 18 January 2010 and right column plots are for 23 December 2009. Several “streaky” vertical features are visible in the group ranges during each event, some of

which extend down to ~ 130 km at PON and ~ 170 km at RSB, indicating that precipitating particles have high enough energy to reach these altitudes. The apparent “V” shape of these features is indicative of moving structures, consistent with the moving auroral features observed in optical data as well as phase delays in TEC variations between different satellite raypaths. A simple calculation based on Rees [1989] suggests that a minimum energy of 1 keV for precipitating electrons is required to produce ionization at an altitude of 130 km, and a minimum of 500 eV is required to produce oxygen green line emission at 557.7 nm [Shiokawa and Fukunishi, 1990]. Based on these facts, CADI data suggest that the precipitating particles causing the ionization and optical intensifications have



(e)

(e) GPS satellite IPP tracks (220 km) - 11:00 to 15:00 UT

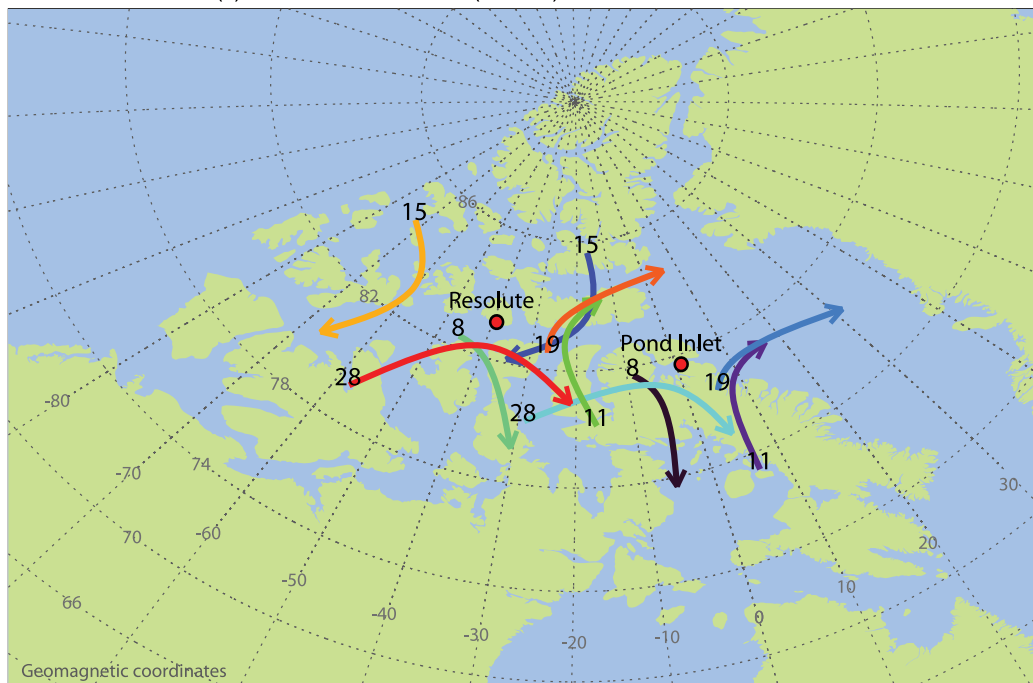


Figure 5. Variations of total electron content (TEC) measured by five GPS satellites (PRNs) at (a) Pond Inlet (PON) and (b) Resolute Bay (RSB) during 11:00–15:00 UT of 23 December 2009. Trend-removed TEC variations at (c) PON and (d) RSB. (e) A map in geomagnetic coordinates of 220 km IPP tracks of the five GPS satellites used in Figures 5a and 5b for the same duration.

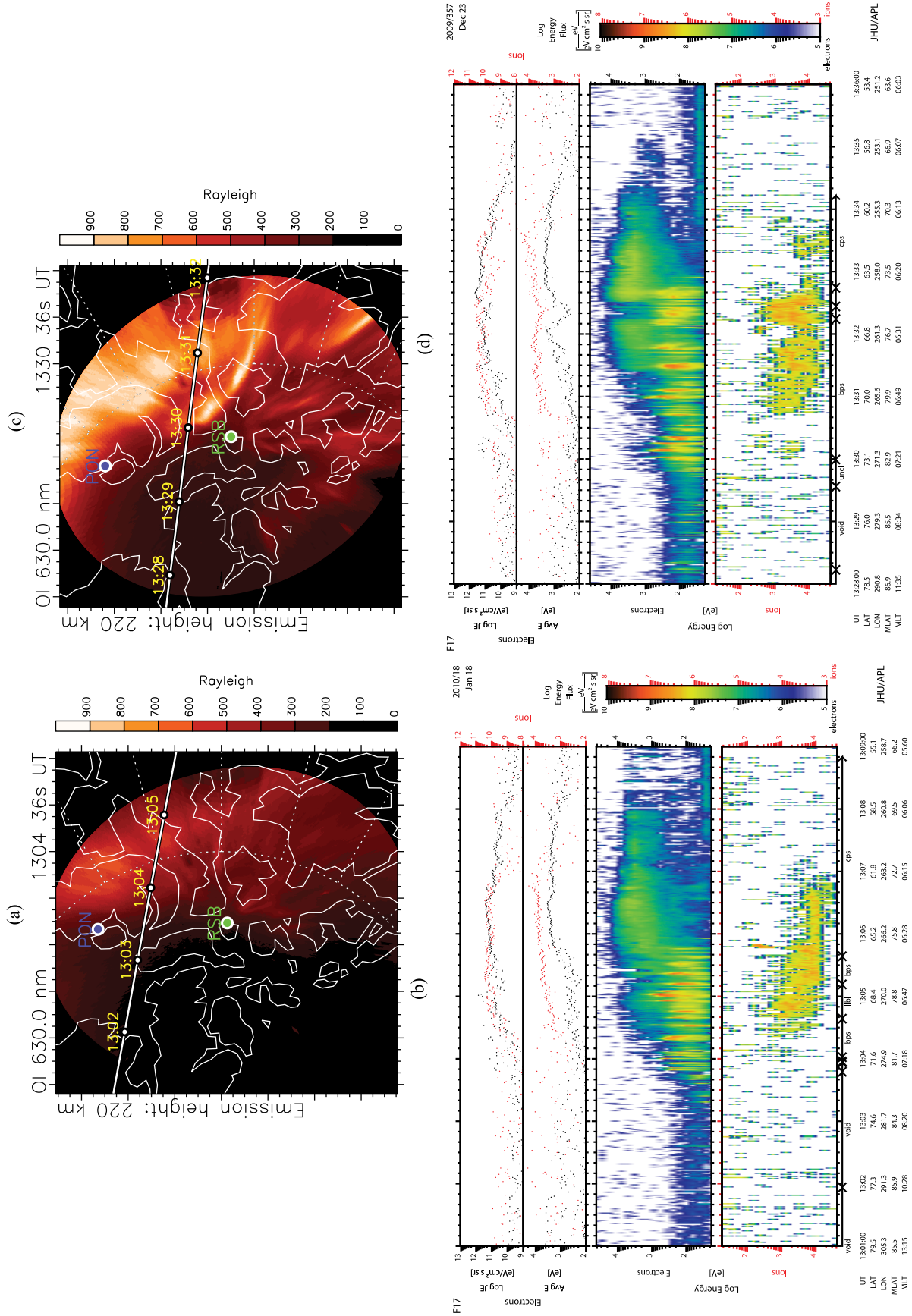


Figure 6

significant energy, which is confirmed by the DMSP data shown in Figure 6.

[10] Figure 7c for 18 January 2010 shows that peak electron density of the ionosphere varied between 1×10^{11} el/m³ and 6×10^{11} el/m³ for PON and between 0.5×10^{11} el/m³ and 2.5×10^{11} el/m³ for RSB, with quasiperiodicity of long and short periods. These electron densities are quite significant for the winter polar cap. Similar to the TEC variations, amplitudes of peak density oscillations at PON are much higher than at RSB since the auroral arcs are closer to PON. One important factor to note is that the electron density shown in the diagram is the maximum electron density, which can come from either the upper *E* region or *F* region. One should use the height (group range) information provided in Figures 7a and 7b for interpreting the electron density variations. For example, some of the large-amplitude variations just after 12:00 UT at PON are for the upper *E* region (~ 130 km) of the ionosphere. For RSB, the lowest reflection height was ~ 170 km, and therefore most of the ionosphere is in the *F* region and the amplitudes of oscillations are much smaller. This again is indicative of the changes in the characteristics of the arc as it moved poleward from the source/generation region. These large-amplitude electron density variations slightly after 12:00 UT at PON correspond to large-amplitude TEC oscillations (~ 2 TECU) recorded by the PON GPS receiver (Figure 3c), whereas the TEC oscillations recorded by the RSB GPS receiver reach only ~ 1.5 TECU.

[11] The right column of Figure 7 shows the group range at 4 MHz measured by CADI at PON (Figure 7d) and RSB (Figure 7e) during the interval 11:00–15:00 UT of 23 December 2009. Vertical “streaks” are again observed, indicating structures present in the lower ionosphere. These streaks started appearing slightly after 11:00 UT, the same time as optical features (Figure 4) and TEC oscillations (Figure 5). Some of these initial (11:15–12:00 UT) vertical streaks reached as low as 140 km at PON and RSB and show “V” type structuring indicative of motion. Peak electron density is shown in Figure 7f, which varied between 1.8×10^{11} el/m³ and 6×10^{11} el/m³ at PON and between 1.3×10^{11} el/m³ and 4.5×10^{11} el/m³ at RSB. The highest-amplitude variations were again observed at PON. An interesting feature of this event is the dramatic change in characteristics of observed features slightly after 13:30 UT. A close examination of group ranges (Figures 7d and 7e) reveals that the vertical streaks after 13:30 UT are confined to *F* region altitudes. This is accompanied by confinement of auroral arcs to regions equatorward of RSB (Figure 4) and a reduction in amplitude and frequency of occurrence of TEC variations (Figures 5c and 5d). Peak electron density for this event is shown in Figure 7f, which varied between 1.8×10^{11} el/m³ and 6×10^{11} el/m³ at PON and between 1.3×10^{11} el/m³ and 4.5×10^{11} el/m³ at RSB. Peak density variations are again higher at PON than at RSB, consistent with the formation of PMSAAs around PON. Ionosonde measurements presented here show that some PMSAA-

associated electron density enhancements occur in the upper *E* region and in the *F* region, indicating significant variation/modulation in the energy of precipitating particles that results in optical intensifications and electron density/TEC enhancements.

[12] The quasiperiodic nature of TEC fluctuations, electron density, and optical features of PMSAAs shown in this paper is quite obvious. Since there seem to be several periodicities in the TEC and electron density variations, it may be useful to identify these frequencies using spectral analysis of 1 Hz TEC measurements. The high sampling rate of GPS observables has made it possible to identify higher-frequency components of TEC oscillations associated with PMSAAs for the first time. Since the cadence of optical measurements is only 2 min and that of electron density measurements by the ionosonde is only 1 min, we are excluding them from this analysis. Figure 8 shows examples of frequency components of TEC fluctuations using the S transform [Stockwell et al., 1996; Mansinha et al., 1997]. PRNs 11 and 29 are chosen as examples because they were the only GPS satellites with more or less continuous measurements of TEC during the entire interval of interest. Figures 8a and 8b show the frequency spectrums of TEC variations from PRN 11 at PON and RSB for the event of 18 January 2010, while Figures 8c and 8d show frequency power spectrums from PRN 28 at PON and RSB for the event of 23 December 2009. The spectrums show several frequency components present in the oscillations starting from the lowest frequency of ~ 1.3 mHz and a maximum frequency of 22.6 mHz. Some of the components are broadband and some are harmonics of 1.3 mHz. Similar discrete frequency components were present in the TEC oscillations along other raypaths. Dominant average (of all raypaths) discrete frequency components seen in the data are 1.6 mHz, 2.6 mHz, 4.03 mHz, 8.53 mHz, 10.97 mHz, 13.45 mHz, and 22.80 mHz. Some of the lower frequencies are also present in optical intensity and electron density measurements; however, higher-frequency components cannot be resolved due to the lower sampling rate. Some of the lower frequencies observed in the TEC data are similar to the ULF wave frequencies observed at these latitudes [e.g., Ziesolleck and McDiarmid, 1995; Baker et al., 2003]. However, the presence of higher frequencies in the TEC data is a new observation and is not usually observed in ground-based magnetometer data [e.g., Baker et al., 2003]. The relationship between different frequencies of TEC oscillations and the electron acceleration observed by DMSP may not be coincidental. It has been shown previously that dispersive Alfvén waves (DAWs) can accelerate electrons in this region [Chaston et al., 2004, 2007], which is statistically the location where broadband acceleration is dominant [Newell et al., 2009b]. TEC oscillations observed here may be signatures of DAWs, but this requires further study. Another observational fact that supports this hypothesis is a change in the frequency of the oscillation (smaller frequency) when the ionization is confined to the

Figure 6. Representative optical images over plotted with the tracks of DMSP F17 satellites during the two events along with corresponding DMSP particle spectrograms. (a) ASI images at 13:04:36 UT of 18 January 2010 with DMSP F17 track from 13:01 UT to 13:09 UT of 18 January 2010. (b) DMSP F17 particle spectrogram during 13:01–13:09 UT of 18 January 2010. (c) ASI images at 13:30:36 UT of 23 December 2009 with DMSP F17 track from 13:28 UT to 13:36 UT of 23 December 2009. (d) DMSP F17 particle spectrogram during 13:28–13:36 UT of 23 December 2009.

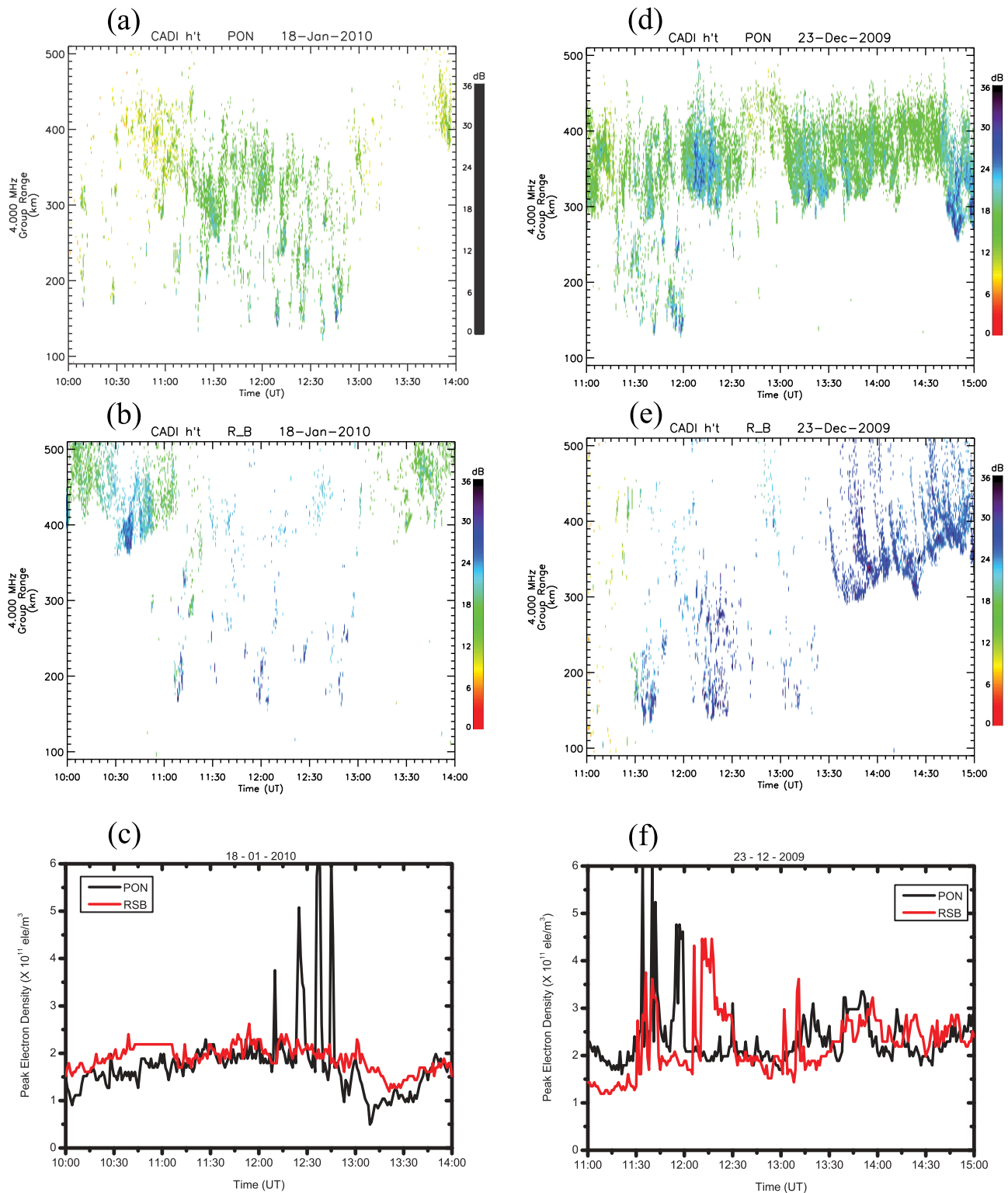


Figure 7. CADI data of group range at 4 MHz and peak electron density of the ionosphere at PON and RSB during the two events. Left column is for the event of 18 January 2010 and the right column is for the event of 23 December 2009. Group ranges at (a) PON and (b) RSB. (c) The variation of peak electron density at PON (black line) and RSB (red line). Group ranges at (d) PON and (e) RSB. (f) The variation of peak electron density at PON (black line) and RSB (red line).

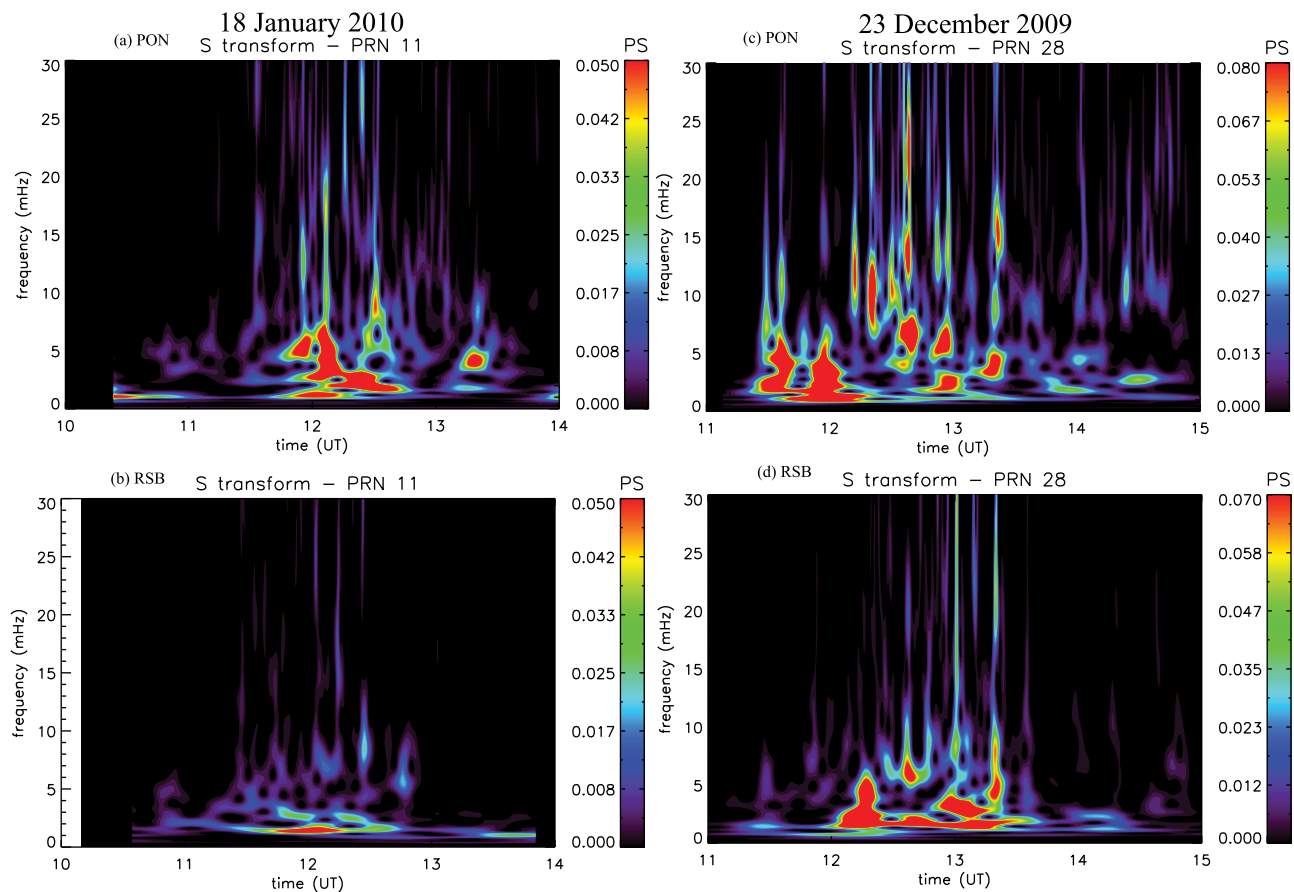


Figure 8. Representative S transform of the GPS TEC measurements from PON and RSB for the two examples presented in this paper. PRN 11 TEC measurements at (a) PON and (b) RSB for the event of 18 January 2010. PRN 28 TEC measurements at (c) PON and (d) RSB for the event of 23 December 2009.

F region (low-energy precipitation), as evident in the case of 23 December 2009 event after 13:30 UT (Figure 5, Figures 6d and 6e, and Figures 8c and 8d). Results presented here show the capability of high data rate TEC measurements in detecting these oscillations, and how TEC can complement other measurements such as magnetometers in studying ULF waves and their role in particle acceleration.

[13] Since we have multiple measurements available, it will be possible to estimate the equivalent vertical thickness of these arcs using the method adopted by Jayachandran *et al.* [2009a]. This method uses the peak electron density measured by the ionosonde and assumes that the electron density is uniform in the vertical direction within the arc. GPS raypaths intersect the arc at an angle and detect a certain increase in TEC. We then can use the peak electron density measured by the CADI and calculate what the vertical thickness of the arc would be in order to provide the observed TEC variation. We can minimize the error in this method using multiple GPS raypaths. Figure 9a shows the distribution of the equivalent vertical thickness of the arcs for both events. The thickness shows a broad distribution between 21 km and 84 km with a mean thickness of 49 km. The only other study regarding vertical thickness of auroral forms that we are aware of is the one by Currie and Weaver [1955] for auroral regions using optical triangulation

methods. They showed a distribution that varied between 20 and 40 km and rarely exceeded 50 km. This upper limit is different from our estimates of the vertical thickness distribution shown in Figure 9a. One obvious reason for the discrepancy may be the fact that Currie and Weaver [1955] based their study on active auroral forms in the auroral region produced by higher-energy precipitation. One way to check this is to look at the relationship between the bottomside height of the enhanced ionization layer produced by the precipitation and the equivalent vertical thickness of the arc. This is based on the fact that higher energies reach lower heights and produce a more narrow layer of enhanced ionization [Rees, 1989] while smaller energies reach only higher heights and result in a broader ionization profile. Figure 9b shows the scatterplot of equivalent vertical thickness of the arcs estimated using ionosonde and GPS measurements and the minimum group range at 3 MHz (equivalent to the bottom of the ionization profile) measured by the CADI. The figure shows a linear relationship between the equivalent vertical thickness of the arc and the bottomside height of the layer. The arc thickness increases linearly with bottom height of the layer, indicating that higher-energy precipitation produces thinner arcs, which is also shown by Rees [1989]. One point to keep in mind is that our vertical thickness estimation is based on an assumption that

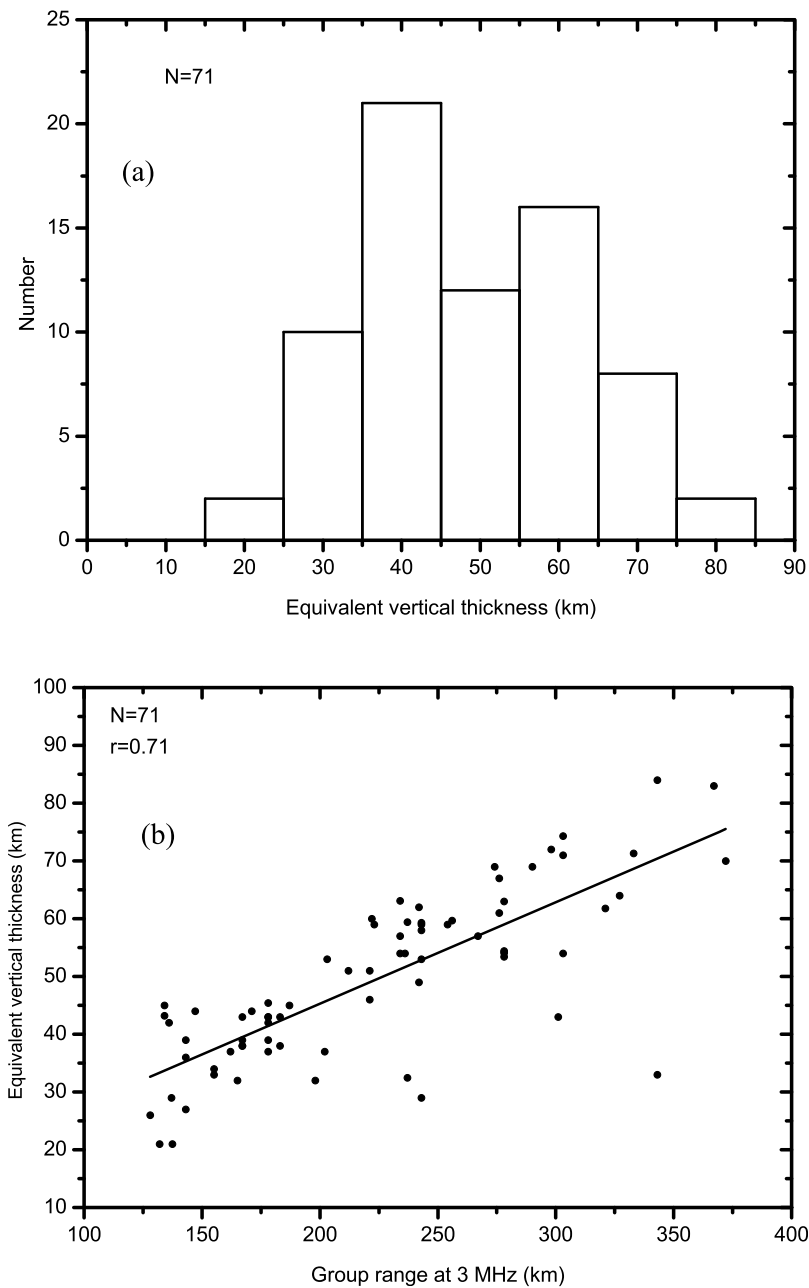


Figure 9. (a) Distribution of equivalent vertical thickness of the arcs estimated using Canadian Advanced Digital Ionosonde (CADI) electron density and GPS TEC measurements. (b) Scatterplot showing the relationship between the group range at 3 MHz (bottom height of the ionosphere) and the estimated equivalent vertical thickness of the arcs.

the peak electron density determined by the ionosonde is uniform within the arc.

5. Summary

[14] Observations of GPS TEC variations associated with PMSAAs showed the following features:

[15] 1. Quasiperiodic TEC variations on the order of ~ 3 TECU showed a decrease in amplitude of variations as the optical forms moved poleward from the source regions.

[16] 2. Simultaneous DMSP data showed that TEC variations and optical intensifications were caused by

precipitation of high-energy (>500 eV) electron precipitation. The source region of precipitation was the boundary plasma sheet, as identified by *Newell and Meng* [1994].

[17] 3. Concurrent ionosonde observations showed similar variations (within the resolution of the data) in peak ionospheric electron density.

[18] 4. The height of ionization layers varied between 130 km (upper *E* region) and 300 km (*F* region), indicating variations in the energy of precipitating particles.

[19] 5. Frequency analysis of high-resolution TEC data showed a broad range of discrete frequency components from 1.6 mHz to 22.80 mHz present in the TEC oscillations,

which may play a role in the energization/modulation of precipitating particles.

[20] 6. Equivalent vertical thickness of arcs estimated using GPS TEC and ionosonde electron density measurements showed a broad distribution with a minimum of 21 km, a maximum of 84 km, and an average of 49 km.

[21] 7. Equivalent vertical thickness of arcs showed a linear relationship with bottomside height of enhanced ionization layers, where an increase in bottomside height corresponded to an increase in vertical thickness. This relationship is a consequence of variations in the energy of precipitating particle, which changes the ionization production profiles.

[22] **Acknowledgments.** Infrastructure funding for CHAIN was provided by the Canada Foundation for Innovation (CFI) and the New Brunswick Innovation Foundation (NBIF). Operation of CHAIN is conducted in collaboration with the Canadian Space Agency (CSA). Part of science funding is provided by the Natural Sciences and Engineering Research Council (NSERC) of Canada. This work was supported by Grants-in-Aid for Scientific Research (16403007, 19403010, and 20244080) from the Japan Society for the Promotion of Science (JSPS). We thank Y. Katoh, M. Satoh, Y. Yamamoto, and Y. Hamaguchi of Solar-Terrestrial Environment Laboratory (STEL), Nagoya University, and SRI International for their helpful support in airglow imaging observations at Resolute Bay. One of the authors (P.T.J.) thanks STEL of Nagoya University for their hospitality during his stay at STEL.

[23] Robert Lysak thanks the reviewers for their assistance in evaluating this paper.

References

- Baker, G. J., E. F. Donovan, and B. J. Jackel (2003), A comprehensive survey of auroral latitude Pc5 pulsation characteristics, *J. Geophys. Res.*, *108*(A10), 1384, doi:10.1029/2002JA009801.
- Basu, S., and C. Valladares (1999), Global aspects of plasma structures, *J. Atmos. Sol. Terr. Phys.*, *61*, 127–139, doi:10.1016/S1364-6826(98)00122-9.
- Chaston, C. C., J. W. Bonnell, C. W. Carlson, J. P. McFadden, R. E. Ergun, R. J. Strangeway, and E. J. Lund (2004), Auroral ion acceleration in dispersive Alfvén waves, *J. Geophys. Res.*, *109*, A04205, doi:10.1029/2003JA010053.
- Chaston, C. C., C. W. Carlson, J. P. McFadden, R. E. Ergun, and R. J. Strangeway (2007), How important are dispersive Alfvén waves for auroral particle acceleration?, *Geophys. Res. Lett.*, *34*, L07101, doi:10.1029/2006GL029144.
- Crowley, G. (1996), Critical review of ionospheric patches and blobs, in *Review of Radio Science 1993–1996*, edited by W. R. Stone, pp. 619–648, Oxford Univ. Press, Oxford, U. K.
- Currie, B. W., and J. T. Weaver (1955), Vertical extent of auroral arcs and bands, *Can. J. Phys.*, *33*(11), 611–617, doi:10.1139/p55-076.
- Davis, T. N. (1960), The morphology of the polar aurora, *J. Geophys. Res.*, *65*, 3497–3500, doi:10.1029/JZ065i010p03497.
- Denholm, J. V., and F. R. Bond (1961), Orientation of polar auroras, *Aust. J. Phys.*, *14*, 193–195, doi:10.1071/PH610193.
- Foster, J. C., et al. (2005), Multiradar observations of the polar tongue of ionization, *J. Geophys. Res.*, *110*, A09S31, doi:10.1029/2004JA010928.
- Frank, L. A., et al. (1986), The theta aurora, *J. Geophys. Res.*, *91*, 3177–3224, doi:10.1029/JA091iA03p03177.
- Hardy, D. A. (1984), Intense fluxes of low-energy electrons at geomagnetic latitudes above 85°, *J. Geophys. Res.*, *89*, 3883–3892, doi:10.1029/JA089iA06p03883.
- Hosokawa, K., K. Shiokawa, Y. Otsuka, A. Nakajima, T. Ogawa, and J. D. Kelly (2006), Estimating drift velocity of polar cap patches with all-sky airglow imager at Resolute Bay, Canada, *Geophys. Res. Lett.*, *33*, L15111, doi:10.1029/2006GL026916.
- Hosokawa, K., T. Kashimoto, S. Suzuki, K. Shiokawa, Y. Otsuka, and T. Ogawa (2009), Motion of polar cap patches: A statistical study with all-sky airglow imager at Resolute Bay, Canada, *J. Geophys. Res.*, *114*, A04318, doi:10.1029/2008JA014020.
- Ismail, S., D. D. Wallis, and L. L. Cogger (1977), Characteristics of polar cap Sun-aligned arcs, *J. Geophys. Res.*, *82*, 4741–4749, doi:10.1029/JA082i029p04741.
- Jayachandran, P. T., K. Hosokawa, J. W. MacDougall, S. Mushini, R. B. Langley, and K. Shiokawa (2009a), GPS total electron content variations associated with a polar cap arc, *J. Geophys. Res.*, *114*, A12304, doi:10.1029/2009JA014916.
- Jayachandran, P. T., et al. (2009b), Canadian High Arctic Ionospheric Network (CHAIN), *Radio Sci.*, *44*, RS0A03, doi:10.1029/2008RS004046.
- Jayachandran, P. T., C. Watson, I. J. Rae, J. W. MacDougall, D. W. Danskin, R. Chadwick, T. D. Kelly, P. Prikryl, K. Meziene, and K. Shiokawa (2011), High-latitude GPS TEC changes associated with a sudden magnetospheric compression, *Geophys. Res. Lett.*, *38*, L23104, doi:10.1029/2011GL050041.
- Kintner, P. M., H. Kil, C. Deehr, and P. Schuck (2002), Simultaneous total electron content and all-sky camera measurements of an auroral arc, *J. Geophys. Res.*, *107*(A7), 1127, doi:10.1029/2001JA000110.
- Kintner, P. M., B. M. Ledvina, and E. R. de Paula (2007), GPS and ionospheric scintillations, *Space Weather*, *5*, S09003, doi:10.1029/2006SW000260.
- Lanzerotti, L. J. (2001), Space weather effects on technologies, in *Space Weather, Geophys. Monogr. Ser.*, vol. 125, edited by P. Song, H. J. Singer, and G. L. Siscoe, pp. 11–22, AGU, Washington, D. C., doi:10.1029/GM125.
- MacDougall, J., and P. T. Jayachandran (2007), Polar patches: Auroral zone precipitation effects, *J. Geophys. Res.*, *112*, A05312, doi:10.1029/2006JA011930.
- Mansinha, L., R. G. Stockwell, R. P. Lowe, M. Eramian, and R. A. Schincariol (1997), Local S-spectrum analysis of 1-D and 2-D data, *Phys. Earth Planet. Inter.*, *103*, 329–336, doi:10.1016/S0031-9201(97)00047-2.
- Newell, P. T., and C.-I. Meng (1994), Ionospheric projections of magnetospheric regions under low and high solar wind pressure conditions, *J. Geophys. Res.*, *99*, 273–286, doi:10.1029/93JA02273.
- Newell, P. T., K. Liou, and G. R. Wilson (2009a), Polar cap particle precipitation and aurora: Review and commentary, *J. Atmos. Sol. Terr. Phys.*, *71*, 199–215, doi:10.1016/j.jastp.2008.11.004.
- Newell, P. T., T. Sotirelis, and S. Wing (2009b), Diffuse, monoenergetic, and broadband aurora: The global precipitation budget, *J. Geophys. Res.*, *114*, A09207, doi:10.1029/2009JA014326.
- Rees, M. H. (1989), *Physics and Chemistry of the Upper Atmosphere*, Cambridge Univ. Press, Cambridge, U. K.
- Sandholt, P. E., and C. J. Farrugia (1999), On the dynamic cusp aurora and IMF B_y , *J. Geophys. Res.*, *104*(A6), 12,461–12,472, doi:10.1029/1999JA900126.
- Sandholt, P. E., M. Lockwood, T. Oguti, S. W. H. Cowley, K. S. C. Freeman, B. Lybekk, A. Egeland, and D. M. Willis (1990), Midday auroral breakup events and related energy and momentum transfer from the magnetosheath, *J. Geophys. Res.*, *95*(A2), 1039–1060, doi:10.1029/JA095iA02p01039.
- Shiokawa, K., and H. Fukunishi (1990), Dependences of auroral 5577 Å and 6300 Å emission rates on thermosphere density variations, *Proc. NIPR Symp. Upper Atmos. Phys.*, *3*, 24–31.
- Shiokawa, K., K. Yumoto, N. Nishitani, K. Hayashi, T. Oguti, D. J. McEwen, Y. Kiyama, F. J. Rich, and T. Mukai (1996), Quasiperiodic poleward motions of Sun-aligned auroral arcs in the high-latitude morning sector: A case study, *J. Geophys. Res.*, *101*, 19,789–19,800, doi:10.1029/96JA01202.
- Shiokawa, K., T. Ogino, K. Hayashi, and D. J. McEwen (1997), Quasiperiodic poleward motions of morningside Sun-aligned arcs: A multievent study, *J. Geophys. Res.*, *102*, 24,325–24,332, doi:10.1029/97JA02383.
- Shiokawa, K., Y. Katoh, M. Satoh, M. K. Ejiri, T. Ogawa, T. Nakamura, T. Tsuda, and R. H. Wiens (1999), Development of optical mesosphere thermosphere imagers (OMTI), *Earth Planets Space*, *51*, 887–896.
- Stockwell, R. G., L. Mansinha, and R. P. Lowe (1996), Localization of the complex spectrum: The S transform, *IEEE Trans. Signal Process.*, *44*, 998–1001, doi:10.1109/78.492555.
- Tsunoda, R. T. (1988), High-latitude F region irregularities: A review and synthesis, *Rev. Geophys.*, *26*, 719–760, doi:10.1029/RG026i004p00719.
- Valladares, C. E., and H. C. Carlson Jr. (1991), The electrodynamic, thermal, and energetic character of intense Sun-aligned arcs in the polar cap, *J. Geophys. Res.*, *96*, 1379–1400, doi:10.1029/90JA01765.
- Valladares, C. E., H. C. Carlson Jr., and K. Fukui (1994), Interplanetary magnetic field dependency of stable Sun-aligned polar cap arcs, *J. Geophys. Res.*, *99*, 6247–6272, doi:10.1029/93JA03255.
- Watson, C., P. T. Jayachandran, E. Spanswick, E. F. Donovan, and D. W. Danskin (2011), GPS TEC technique for observation of the evolution of substorm particle precipitation, *J. Geophys. Res.*, *116*, A00190, doi:10.1029/2010JA015732.
- Zhu, L., R. W. Schunk, and J. J. Sojka (1997), Polar cap arcs: A review, *J. Atmos. Sol. Terr. Phys.*, *59*, 1087–1126, doi:10.1016/S1364-6826(96)00113-7.
- Ziesolleck, C. W. S., and D. R. McDiarmid (1995), Statistical survey of auroral latitude Pc 5 spectral and polarization characteristics, *J. Geophys. Res.*, *100*, 19,299–19,312, doi:10.1029/95JA00434.